ChemPhotoChem
Research Article
doi.org/10.1002/cptc.202300171
Chemistry Europe
European Chemical Societies Publishing
www.chemphotochem.org

Special Collection

# An Indolin-3-imine Photobase and pH Sensitive Fluorophore

Susanne Doloczki,[a] Christoph Kern,[a] Karl O. Holmberg,[b] Miao Zhao,[b] Fredrik J. Swartling,[b] Jan Streuff,[a] and Christine Dyrager*[a]

This work presents the pH sensing ability of a fluorescent indolin-3-imine derivative. Protonation of the weakly basic imine (p$K_a$ = 8.3 of its conjugate acid) results in a significant red-shift of the absorption band. The fluorophore acts as a photobase, with a basicity increase of approximately 6 units upon photoexcitation. This behavior promotes excited state proton transfer from weak acids such as protic solvents. The characteristics of the fluorophore enable sensing of water fractions in organic solvents and differentiation between methanol, ethanol, and longer chain alcohols. Initial cell studies indicated the future potential of indolin-3-imines as fluorophores for bioimaging applications.

## Introduction

Optical pH sensors are crucial tools in environmental, material, and life sciences.[1] The ability to monitor pH or proton transfer in biological systems is especially important because these govern vital functions and chemical reactions in living systems.[1c,2] Fluorescent pH sensitive compounds are commonly used in bioimaging,[3] for instance, to stain acidic organelles or to probe dysregulated extra/intracellular pH – a feature of various types of cancer.[4]

The pH sensing mechanism of emissive compounds, caused by protonation, usually relies on the following effects: i) suppression of photoinduced electron transfer (*i.e.*, turn-on fluorescence),[5] ii) extension of electron conjugation by rearrangement,[6] or iii) change of the electronics of donor-acceptor fluorophores.[7] Some molecules (weak acids or bases) act as sensors due to excited state proton transfer (ESPT); a feature that is enabled by their increased acidity/basicity upon excitation.[8] Such photoacids/photobases, have attracted attention due to the prospect of exploiting their properties in various valuable applications.[9] These include photocurrent generation,[10] light-mediated polymerization[11] and enantioselective protonation of silyl enol ethers, which allows for stereospecific synthesis of α-substituted carbonyls.[12]

In this work, we studied the photophysical properties and pH sensing ability of an indolin-3-imine derivative, **Ind** (Figure 1A), which has previously only been described as fluorescent in literature.[13] This structure consists of an electron-donating cyclic amine, which is conjugated through a fused aromatic ring to an electron-withdrawing imine moiety. The donor-acceptor characteristics of **Ind** allows for intramolecular charge transfer in the excited state, which results in increased basicity of the imine group, thus creating a photobase. To the best of our knowledge, this is the first study exploring the photophysical characteristics of indolin-3-imines, including their utility as pH-probes, photobases and their potential as emissive agents for fluorescence cell microscopy.

## Results and Discussion

### Solvent Effects on UV-Vis Absorption Spectra

The photophysical properties of **Ind** were initially investigated in toluene, DMSO and methanol (Figures 1A–C). The lowest energy absorption maximum ($\lambda_{Amax}$) shifted bathochromically with increasing solvent polarity (from 365 nm in toluene to 443 nm in methanol) (Figure 1B and ESI, Figure S1). Positive solvatochromism of the absorption in aromatic compounds can often be attributed to π–π* transitions when the dipole moment of the excited state is considerably larger than that of the ground state.[14] In methanol, two absorption bands were observed ($\lambda_{Amax}$ = 400 and 443 nm), which exhibited concentration-dependent intensity ratios (Figure 1D). For clarity of discussion, from this point forward, the absorption band at the shorter wavelength is referred to as the A-band and the band at the longer wavelength is referred to as the B-band (regardless of solvent), as indicated in Figure 1B.

Increasing the concentration of **Ind** in methanol increased the A-band/B-band intensity ratio (Figure 1D), which could indicate the presence of aggregates. The opposite effect was

[a] S. Doloczki, C. Kern, Prof. Dr. J. Streuff, Dr. C. Dyrager
Department of Chemistry – BMC
Uppsala University
Box 576, 75123 Uppsala (Sweden)
E-mail: christine.dyrager@kemi.uu.se

[b] Dr. K. O. Holmberg, Dr. M. Zhao, Dr. F. J. Swartling
Department of Immunology, Genetics and Pathology
Uppsala University
Rudbeck Laboratory, 75185 Uppsala (Sweden)

*Supporting information for this article is available on the WWW under https://doi.org/10.1002/cptc.202300171*

*Part of a Special Collection celebrating the 140th anniversary of the Swedish chemical society.*

Research Article
doi.org/10.1002/cptc.202300171


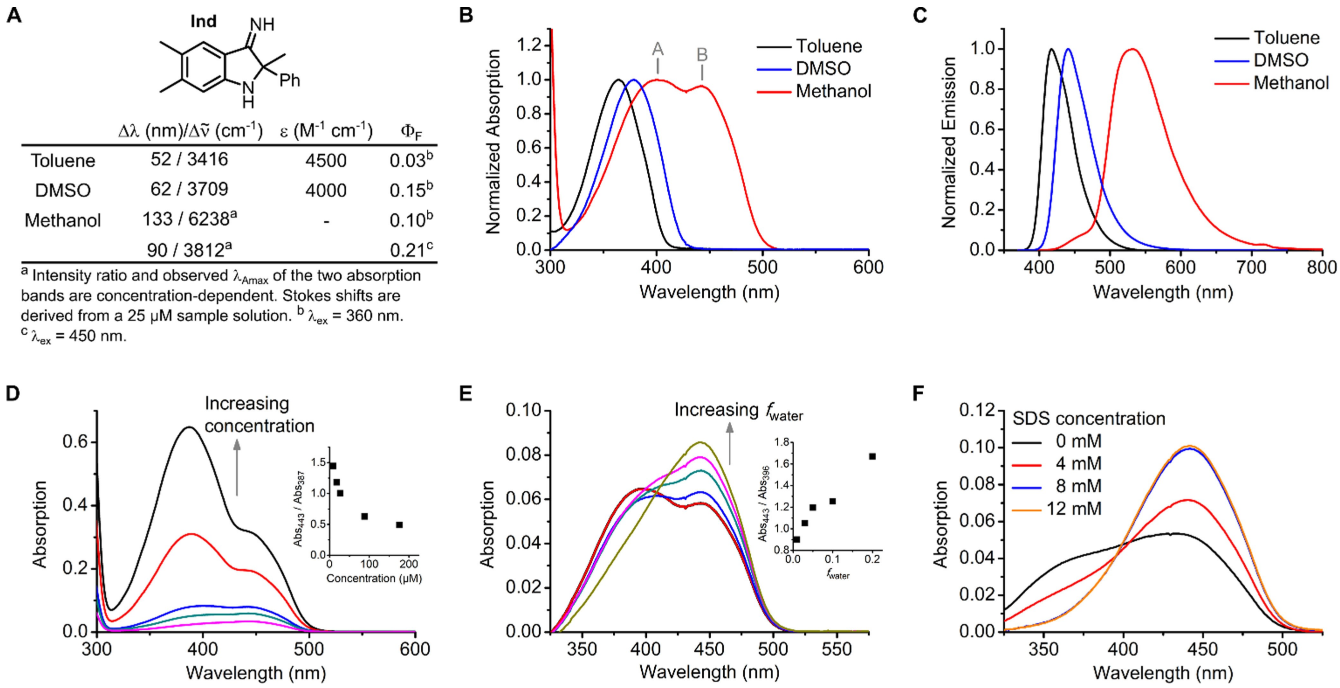


**Figure 1.** Photophysical data of **Ind** in different solvents (A–C) and the influence of concentration (D), water fraction (E), and surfactant (F) on its absorption spectra. A) Summary of Stokes shifts ($\Delta\lambda$ and $\Delta\tilde{\nu}$), molar extinction coefficients ($\varepsilon$) and fluorescence quantum yields ($\Phi_F$). B) Normalized absorption spectra. The two absorption bands in methanol are labelled as A-band and B-band, respectively. C) Normalized emission spectra ($\lambda_{ex}=360$ nm). D) Influence of concentration (9–176 μM) on the absorption spectra of **Ind** in methanol. The B-band dominates at low concentrations, whereas the A-band dominates at high concentrations; inset: B-band/A-band absorbance ratio plotted against the concentration. E) Effect of water fraction on the absorption spectra of **Ind** in methanol. The B-band of **Ind** (25 μM) becomes more pronounced with increasing volume fraction of water ($f_{water}$; 0–0.2); inset: B-band/A-band absorbance ratio plotted against $f_{water}$. F) Effect of the anionic surfactant sodium dodecyl sulfate (SDS) on the absorption spectra of **Ind** (20 μM) in water (with 5% DMSO). The B-band becomes more pronounced with increasing SDS concentration.

observed with increasing water fractions in methanol (Figure 1E). Intrigued by these results, additional experiments were performed in DMSO-water solvent mixtures. A red-shifted absorption band (around 450 nm) appeared, which also increased in intensity, when increasing the volume fractions of water (ESI, Figure S2). Methanol had a similar but less significant effect on **Ind** in DMSO than water (ESI, Figure S2), whereas the addition of methanol to **Ind** in toluene merely caused a bathochromic shift of the absorption band (ESI, Figure S1); no additional absorption band was observed. The logarithmic growth of the red-shift, with increasing amounts of methanol, resembles the trend of $E_T(30)$ solvent polarity in toluene-methanol binary mixtures.[15] Based on the absorption spectroscopy results, we hypothesized that **Ind** participates in a ground state equilibrium in polar protic solvent systems, likely involving proton transfer (*i.e.*, acid-base equilibrium or tautomerism).

### Influence of Additives on the Acid–Base Equilibrium

Addition of surfactants is known to influence acid-base equilibria, with anionic surfactants stabilizing cationic species in solution.[16] Surfactants can also form micelles and affect the degree of aggregation. The equilibrium of **Ind1** in water (with 5% DMSO) shifted to the B-band species when the anionic surfactant sodium dodecyl sulfate (SDS) was added (Figure 1F). In addition to our other observations, the B-band can therefore likely be ascribed to the cationic/protonated form of **Ind**. To further test this hypothesis, an excess of acid (aq. HCl) or base (aq. NaOH) was added to solutions of **Ind** in MeOH or DMSO. In both solvents, the equilibrium shifted completely to the B-band in the presence of acid and to the A-band in the presence of base (ESI, Figure S3). This strongly indicates that the B-band corresponds to the absorption of the protonated compound (**IndH**$^+$) and that the A-band most likely corresponds to the neutral **Ind**. It was noted that the B-band species exhibits slightly higher molar absorptivity than the A-band species, e.g., 1.2 times higher in methanol with excess acid or base ($\varepsilon=4.7$ and $3.9\times10^3$ $M^{-1}cm^{-1}$, respectively). NMR spectroscopy experiments confirmed that stoichiometric addition of aq. HCl to **Ind** in DMSO-$d_6$ resulted in protonation of the imine (ESI, Figures S13–S17). Finally, the p$K_a$ of **IndH**$^+$ was spectrophotometrically determined to be 8.3 in aqueous solution (Figures 2A–C). Upon protonation in Britton-Robinson-buffer, the red-shift of absorption amounted to 74 nm (4641 $cm^{-1}$). In basic solutions, a considerable decrease of emission intensity was observed.

### Fluorescence Spectroscopy

By analogy to $\lambda_{Amax}$, the emission maxima ($\lambda_{Emax}$) of **Ind** shifted bathochromically with increasing solvent polarity (Figure 1C). The Stokes shifts are quite large (52–90 nm, 3.4–3.8×10$^3$ $cm^{-1}$)

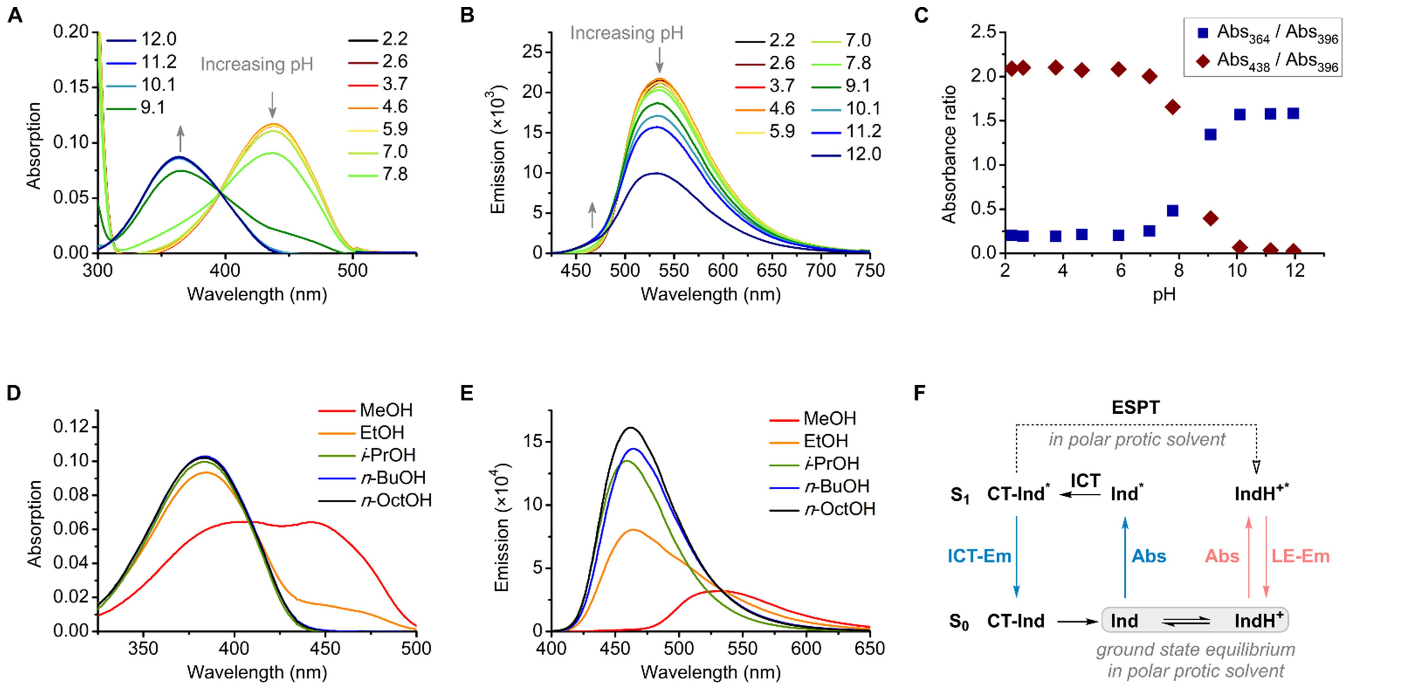


**Figure 2.** Influence of solvent acidity on **Ind** (A–E) and proposed photophysical processes of **Ind** (F). A–B) pH-Dependence of absorption (A) and emission spectra (B; $\lambda_{ex} = 396$ nm) of **Ind** (25 μM) in Britton–Robinson buffer (with 1 % DMSO). C) pH Curves based on the absorbance ratio of **Ind** or **IndH**$^+$ ($\lambda = 364$ or 438 nm) and the isosbestic point ($\lambda = 396$ nm). D–E) Absorption (D) and emission spectra (E) of **Ind** (25 μM) in different alcohols (methanol, ethanol, *i*-propanol, *n*-butanol, *n*-octanol); $\lambda_{ex} = 384$ nm or 404 nm (MeOH). F) Proposed ground and excited state processes of **Ind** in polar protic solution. Abs = absorption; Em = emission; ESPT = excited state proton transfer; ICT = intramolecular charge transfer; LE = locally excited; $S_0$ = singlet ground state; $S_1$ = first singlet excited state.

and the fluorescence quantum yields ($\Phi_F$) range from 0.03–0.15, with the lowest value obtained from measurements in toluene. Importantly, and in the light of our recent publication of the photolabile ketone analogue of **Ind**,[17] it should be emphasized that **Ind** features high photostability (ESI, Figure S7).

Individual excitation of the two absorption bands ($\lambda_{ex} = 360$ or 450 nm, respectively) in methanol resulted in very similar emission spectra with $\lambda_{Emax} = 533$ nm (ESI, Figure S4). The difference between the spectra was the presence of a weak shoulder at *ca.* 460 nm when the shorter excitation wavelength was used ($\lambda_{ex} = 360$ nm). This weak shoulder did not appear at $\lambda_{ex} =$ 450 nm. Analysis of the excitation spectra confirmed that only the A-band contributes to the shoulder, whereas both absorption bands contribute to the major emission band (ESI, Figure S4). Based on these observations, we propose that different processes take place, as illustrated in Figure 2F. Each species in the ground state acid-base equilibrium can be excited individually. The emission of **IndH**$^+$ originates from the locally excited (LE) state, which is virtually independent of solvent polarity. On the other hand, **Ind** can undergo intramolecular charge transfer (ICT) in the excited state, resulting in solvatochromic emission. In polar protic solvents (such as methanol and water) a competing pathway is available, namely excited state proton transfer (ESPT) from the solvent. The resulting excited state species is identical to **IndH**$^{+*}$. The ESPT most likely occurs from **CT-Ind***. Weak bases that undergo ICT in the excited state typically exhibit an increased excited state basicity. Such compounds are called photobases and the excited state acidity ($pK_a$*) of their conjugate acids can be estimated using the Förster equation and the 0–0 transition energies of both species (neutral and protonated).[8e,18] Accordingly, **Ind** gave an approximate $pK_a$* of 14 (see Experimental Section for details), which constitutes an increase of the acid constant by six orders of magnitude upon photoexcitation. $\Delta pK_a$ ($= pK_a^* - pK_a$) values for other reported photobases typically range between 1 to 14.[18b,19] Photobases that are not protonated in the ground state, but emit from the protonated excited state, can exhibit large apparent Stokes shifts. This approach has therefore been used as strategy to design fluorescent proteins with large Stokes shifts.[20]

## Experiments in Deuterated Solvent and Various Alcohols

Comparison of the UV-vis spectra of **Ind** in methanol and deuterated methanol showed a slight increase of the A-band/B-band intensity ratio in the latter (ESI, Figure S5). This is in accordance with the marginally less acidic nature of deuterated solvents.[21] Furthermore, the emission intensity ratio of the shoulder and the major band increased about 1.7-fold in the deuterated solvent (ESI, Figure S5). This result is in accordance with the expected decelerating isotope effect on the ESPT rate.[22] Although the emission behaves similarly in both solvents, the emission intensity (corrected for differences in absorption intensity) in deuterated methanol was about two times higher. Reduced quenching of fluorescence in deuterated

Research Article
doi.org/10.1002/cptc.202300171


water or deuterated alcohols is a common phenomenon, which recently been systematically investigated.[23] Furthermore, absorption spectra of **Ind** recorded in various aliphatic alcohols revealed that only methanol and, to a lesser extent, ethanol are capable of partially protonating **Ind** (Figures 2D–E and ESI, Figure S6). Solutions of **Ind** in longer chain alcohols (*i*-propanol, *n*-butanol, and *n*-octanol) did not show any red-shifted band (B-band) in their absorption spectra, indicating their acidity is too low or that they cannot sufficiently stabilize $\mathbf{IndH^+}$ due to their lower dielectric constants. Accordingly, ethanol promotes neutral **Ind** as the major species in the ground state and is weaker at promoting proton transfer in the excited state as compared to methanol. As a result, the emission spectrum of **Ind** in ethanol peaks at $\lambda_{Emax} = 464$ nm when excited at the maximum of the A-band ($\lambda_{Amax} = 384$ nm), which is close to the emission maxima that were recorded in the other longer chain alcohols that were examined (Figure 2E). In line with our results, Hunt and Dawlaty have shown that the rate of ESPT of the photobase 5-methoxyquinoline in alcohols is dependent on solvent acidity, with more acidic alcohols increasing the rate.[24] Furthermore, the behavior of **Ind** in alcohols is similar to other reported fluorophores with imine moieties.[7c,25] Deprotonation of alcohols may be explained by the empirical p$K_a$ rule.[26] Accordingly, weak bases can be protonated if the p$K_a$ of their conjugate acids and the protonation source (e.g. a weak acid such as MeOH or EtOH) do not differ by more than 8 units.

### Computational Studies

Density functional theory (DFT) and time-dependent DFT (TDDFT) calculations were performed to compute the vertical transitions of **Ind** and $\mathbf{IndH^+}$ (ESI, Table S2). The mean absolute errors of **Ind** (toluene, MeOH; PCM) and $\mathbf{IndH^+}$ (MeOH; PCM) were between 0.20–0.37 eV compared to the experimental absorption values. Furthermore, the computed difference in absorption energy between **Ind** and $\mathbf{IndH^+}$ (MeOH; PCM) was comparable to the experimental energy difference of the absorption bands in basified and acidified methanol (calculated 0.35 eV/40 nm *vs.* experimental 0.46 eV/62 nm). All computed transitions represent HOMO-LUMO transitions (ESI, Figure S9). The amine has a strong contribution in the HOMO of the neutral molecule, whereas the LUMO is dominated by the imine. In case of the protonated compound, both frontier molecular orbitals are distributed similarly over the entire conjugated system (including both nitrogen atoms). This supports the experimental evidence of ICT in **Ind** and LE state in $\mathbf{IndH^+}$. Computation of the dearomatized tautomer of **Ind** indicated that it is not energetically accessible in the ground state ($\Delta E = 0.47$ eV $= 10.8$ kcal/mol) and thus likely does not play an important role here.

### Preliminary Cell Studies

Indolin-3-imines have previously not been investigated as imaging probes for cell biology research. The fluorescence cell imaging utility of **Ind** was therefore investigated using (healthy) human dermal fibroblast (HDF) and melanoma cells (SK-MEL-28). The fluorescence of **Ind** could clearly be observed in both cell lines upon excitation using the green laser ($\lambda_{ex} = 488$ nm). The accumulation pattern in melanoma cells seemed rather unspecific, whereas in fibroblasts the compound was preferentially localized in lysosomes (*i.e.*, acidic organelles[27]) (ESI, Figures S10–S11). In addition, **Ind** showed no significant effects on cell viability under the studied conditions (ESI, Figure S12). These preliminary results indicate that indolin-3-imines could be a new promising class of fluorophores for applications within chemical biology, including fluorescence cell imaging.

## Conclusions

We have presented the photophysical properties and pH sensing capability of an indolin-3-imine derivative (**Ind**). Its key characteristics include a significantly red-shifted absorption upon protonation, a relatively high p$K_a$ (8.3) of its conjugate acid and increased basicity upon excitation. These chemical and photophysical properties enable deprotonation and sensing of water fractions in organic solvents. Emission of the protonated species was proposed to occur from the locally excited state, whereas emission of the neutral form occurs after intramolecular charge transfer. The photobasicity of **Ind** further facilitates the deprotonation of weak acidic protic solvents (such as methanol and, partially, ethanol) via ESPT. Initial imaging experiments of **Ind** in melanoma and fibroblast cells indicated its usefulness as a fluorescent probe for bioimaging. This study is the first to investigate the photophysical behavior of **Ind** (or its derivatives). We envisage that it will inspire further investigations of indolin-3-imine derivatives as i) photobases, ii) molecular tools for bioimaging, and iii) general optical sensors for applications where pH sensitivity is of high importance.

## Experimental Section

The synthesis and full characterization of **Ind** has previously been described in detail in the Supporting Information of our preceding paper.[17]

### NMR Spectroscopy

NMR spectra were recorded at 298 K using an Agilent MR400-DD2 instrument at 400 MHz ($^1$H) and 101 MHz ($^{13}$C) or a Bruker Avance Neo instrument at 500 MHz ($^1$H) and 126 MHz ($^{13}$C). Chemical shifts (δ) are reported in ppm using the residual solvent peak in DMSO-$d_6$ ($\delta_H = 2.50$ and $\delta_C = 39.52$ ppm) as internal reference.[28] The apparent resonance multiplicity is reported as s (singlet) or m (multiplet). Experimental details of the protonation experiment are given in the corresponding figure caption (ESI, Figure S13).

### Photophysical Characterization

The following organic solvents were used for photophysical measurements: toluene (ACS grade, VWR chemicals; distilled prior to use), methanol and *i*-propanol (HPLC grade, VWR chemicals), DMSO (Uvasol, Merck/Supelco), ethanol absolute (AnalaR NORMAPUR ACS, VWR chemicals), *n*-octanol (HPLC grade, Sigma-Aldrich), *n*-butanol (p. a., Merck). UV-vis absorption spectra were acquired on a UV-1650PC Shimadzu instrument at room temperature using quartz cuvettes (10 mm). Absorption maxima ($\lambda_{Amax}$) are reported in nm and the molar extinction coefficient ($\varepsilon$) in $M^{-1}\,cm^{-1}$ with a margin of error of up to 1%. At least three data points with different known concentrations were acquired and the measured absorbances ($\leq 1.0$) were plotted against the concentrations. The molar extinction coefficients were then determined according to the Beer-Lambert law as the slope of the linear fit. Fluorescence measurements were carried out using a Shimadzu RF-6000 spectrofluorophotometer. Fluorescence quantum yields ($\Phi_F$) were determined with $\lambda_{ex}=360$ nm relative to quinine sulfate in 0.05 M aq. $H_2SO_4$ ($\Phi_F=0.55$)[29] or with $\lambda_{ex}=450$ nm relative to fluorescein in 0.1 M aq. NaOH ($\Phi_F=0.93$).[29] At least three fluorescence spectra were recorded per solvent, and integrated peak areas were plotted against the absorbances at the excitation wavelength. The quantum yields were then calculated from the slope of the linear fit *via* the comparative method, with a margin of error of up to 4%. The concentrations for the quantum yield measurements were selected so that the absorbance was below 0.1 to prevent inner filter effects. Obtained raw data was processed using OriginPro 8 software.

## p$K_a$ Determination and p$K_a$* Estimation

The Britton-Robinson buffer[30] was prepared by mixing equal volumes of aqueous solutions (all 0.04 M) of acetic acid, boric acid, and phosphoric acid. Solutions with various pH (between 2 and 12) were obtained by addition of aqueous NaOH solution (0.2 M). The pH values were measured using a pH meter (VWR pHenomenal pH 1000 L). A stock solution of **Ind** (2.5 mM) in DMSO was prepared and diluted with each buffer solution to reach a final compound concentration of 25 μM (1% final DMSO content), respectively. Subsequently, the absorption spectrum of each sample solution was recorded, and the data was plotted according to Equation (1), giving the p$K_a$ value of the compound as y-intercept of the linear fit (as previously described by others[31]).

$$pH = pK_a + slope \times log\frac{R - R_{min}}{R_{max} - R} \quad (1)$$

Hereby, $R$ is defined as ratio of absorption intensity at two wavelengths, in this case at 438 nm (acidic maximum) or 364 nm (basic maximum) and at 396 nm (isosbestic point), as can be seen in Figure 2C. $R_{min}$ and $R_{max}$ are the minimum and maximum limits, respectively. Based on this analysis, an error of $\pm 0.1$ is assumed for the determined p$K_a$.

The excited state acidity (p$K_a$*) of **IndH$^+$** was estimated using the Förster equation, Equation (2), as previously described by others.[8e,18]

$$\begin{aligned} pK_a^* &= pK_a + \frac{N_A hc}{2.303RT}\left(\tilde{v}_{00}^{B} - \tilde{v}_{00}^{BH^+}\right) \\ &= pK_a + \frac{0.625\text{Kcm}}{T}\left(\tilde{v}_{00}^{B} - \tilde{v}_{00}^{BH^+}\right) \end{aligned} \quad (2)$$

where $N_A=6.022\times10^{23}\,mol^{-1}$ (Avogadro constant), $h=6.625\times10^{-34}$ Js (Planck constant), $c=3\times10^{10}$ cm (speed of light), $R=8.31\,J\,mol^{-1}K^{-1}$ (gas constant), $T$=temperature in K, $\tilde{v}_{00}^{B}$=0–0 transition energy of base in $cm^{-1}$, $\tilde{v}_{00}^{BH^+}$=0–0 transition energy of conjugate acid in $cm^{-1}$.

The 0–0 transition energies were estimated from the intersection of the absorption and emission spectra in acidic (1 M aq. HCl) or basic (1 M aq. NaOH) solutions (20 μM **Ind**; MeOH was used to help solubilization, final MeOH content: 0.4%; ESI, Figure S8). The following values were obtained: $\tilde{v}_{00}^{B}=23213\,cm^{-1}$, $\tilde{v}_{00}^{BH^+}=20504\,cm^{-1}$.

## Computational Details

All density functional theory (DFT) calculations were performed using Gaussian 09[32] software and PBE1PBE/6-311G(d,p) level of theory for ground states. Time-dependent density functional theory (TDDFT) was applied to excited states at PBE1PBE/6-311+G(2d,p) level of theory.[33] The polarizable continuum model (PCM) was used to account for implicit solvation effects of toluene and methanol. Vertical transitions (at least five excited states) were generally calculated with state-specific solvation. Optimized geometries were confirmed as energetic minimum by vibrational frequency calculations. Computed structures and orbitals were visualized using Avogadro 1.2.0.[34]

## Cell Cultures

SK-MEL-28 (ATCC:HTB-72) and adult Human Dermal Fibroblast (HDF) (Sigma-Aldrich, Cat#106-05 A) cells were grown in Dulbecco's Modified Eagle Medium (DMEM), high glucose, GlutaMAX™ (Thermo Fisher Scientific, Cat#61965026) supplemented with 10% heat inactivated Fetal Bovine Serum (Thermo Fisher Scientific, Cat#10270106) and Penicillin-Streptomycin (Sigma-Aldrich, Cat#P0781) using 100 mm TC treated dishes (VWR, Cat#734-0006) and a humidified incubator at 37 °C with 5% $CO_2$. Cells were passaged using Trypsin – EDTA Solution (Sigma-Aldrich, Cat#T3924) after washing with Dulbecco's Phosphate-Buffered Saline (DPBS) (Thermo Fisher Scientific, Cat#14190094).

## Cell Staining, Colocalization, and Fluorescence Microscopy

SK-MEL-28 and HDF cells were counted using a Countess II Automated Cell Counter (Thermo Fisher Scientific, Cat#A-MQAX1000) and seeded in chamber slides (Sarstedt, Cat#94.6140.802) the day before treatment at 40 000 live cells/well. A stock solution of **Ind** in DMSO (Uvasol, Merck/Supelco) was prepared at 5.0 mM concentration, which was diluted with cell medium to 20 μM final compound concentration (note: 10 μM also works well). Live cells were incubated with the compound for 1 h or 24 h with DMSO treated cells as control (*i.e.*, 0.4 vol% DMSO). The cells were washed with PBS solution, fixed for 15 min at rt in the dark using a 4% Buffered Formaldehyde Solution (Histolab Cat#02176) and further washed with PBS solution prior to mounting with Fluoromount (Sigma-Aldrich, Cat#F4680). Stainings were performed at least twice to ensure reproducibility. Fluorescence imaging was performed using a Zeiss LSM700 confocal microscope with ZEN (black edition) software ($\lambda_{ex}=488$ nm, $\lambda_{em}=500$–700 nm). The acquired raw data was processed using ImageJ (Fiji distribution).[35] Background subtraction, brightness and contrast adjustments were made to improve visibility. For colocalization, a modified literature procedure was followed.[36] The cells were seeded the day before treatment at 20 000 live cells/well. After incubation with **Ind** (20 μM) for 24 h, the cells were washed with cell medium (warmed up to 37 °C) and then incubated with a solution of LysoTracker Deep Red (ThermoFisher Scientific, Cat#L12492) in cell medium (75 nM, 500 μL) for 30 min at 37 °C. Appropriate controls with only **Ind**, LysoTracker Deep Red, or blank DMSO were prepared in parallel. The cells were washed with PBS (2×), followed by fixation and mounting as described above. For imaging, LysoTracker Deep Red was excited at 639 nm and detected using an LP640 filter. **Ind** was excited at 488 nm and detected below 600 nm. The fluorophores were imaged sequentially, and the controls were imaged with the same settings to confirm that no crosstalk of the fluorophores was detected.

### Cell Viability Assay

Cells were counted (as mentioned above) and seeded in 96 well plates the day before treatment at 5000 or 10 000 live cells/well. **Ind** was dissolved in DMSO (Uvasol, Merck/Supelco) and further diluted in extra cell culture medium before cell treatment. Cells were incubated with the compound for 24 h at a final concentration of 10 or 20 μM with DMSO treated cells as control (0.4 vol%). Cell viability was analyzed after 2.5 h incubation with Resazurin Reagent (1:10) (Sigma-Aldrich, Cat#R7017) using a Synergy™ HTX Multi-Mode Reader (BioTek) by measurement of the fluorescence at 590 nm ($\lambda_{ex}=530$ nm) or using a CLARIOstar Plus plate reader (BMG LABTECH) by measurement of the fluorescence at 600 nm ($\lambda_{ex}=544$ nm). At least two independent experiments (in triplicates) were performed.

## Supporting information

The authors have cited additional references within the Supporting information.[37]

## *Acknowledgements*

This work was supported financially by the Swedish Research Council (Dnr: 2018-03524, to C. D.) and the Cusanuswerk (Fellowship to C. K.). NMR spectrometers were provided by the NMR Uppsala infrastructure, which is funded by the Department of Chemistry – BMC and the Disciplinary Domain of Medicine and Pharmacy. We thank Professor Karin Öllinger and Dr. Ida Eriksson for performing pilot studies on additional cell lines and for a helpful discussion regarding lysosomal staining. Furthermore, we thank Mauricio Posada Urrutia for help with the NMR spectrometer, the Department of Medicinal Chemistry for providing the fluorometer, and Dr. Lukasz T. Pilarski for proof-reading the manuscript. We acknowledge the BioVis platform of Uppsala University for providing the confocal microscope. Calculations were performed on resources provided by the Swedish National Infrastructure for Computing (SNIC) at Uppsala Multidisciplinary Center for Advanced Computational Science (UPPMAX), partially funded by the Swedish Research Council through grant agreement no. 2018-05973.

## *Conflict of Interests*

The authors declare no conflict of interest.

## *Data Availability Statement*

The data that support the findings of this study are available from the corresponding author upon reasonable request.

**Keywords:** proton transfer · pH sensors · fluorophores · imaging agents · photobase

[1] a) D. Wencel, T. Abel, C. McDonagh, *Anal. Chem.* **2014**, *86*, 15–29; b) A. Steinegger, O. S. Wolfbeis, S. M. Borisov, *Chem. Rev.* **2020**, *120*, 12357–12489; c) L. Di Costanzo, B. Panunzi, *Molecules* **2021**, *26*, 2952.
[2] T. Gensch, J. Heberle, C. Viappiani, *Photochem. Photobiol. Sci.* **2006**, *5*, 529–530.
[3] a) J. Han, K. Burgess, *Chem. Rev.* **2010**, *110*, 2709–2728; b) H. Zhu, J. Fan, J. Du, X. Peng, *Acc. Chem. Res.* **2016**, *49*, 2115–2126; c) J.-T. Hou, W. X. Ren, K. Li, J. Seo, A. Sharma, X.-Q. Yu, J. S. Kim, *Chem. Soc. Rev.* **2017**, *46*, 2076–2090; d) Y. Yue, F. Huo, S. Lee, C. Yin, J. Yoon, *Analyst* **2017**, *142*, 30–41.
[4] B. A. Webb, M. Chimenti, M. P. Jacobson, D. L. Barber, *Nat. Rev. Cancer* **2011**, *11*, 671–677.
[5] a) L. Wang, Y. Xiao, W. Tian, L. Deng, *J. Am. Chem. Soc.* **2013**, *135*, 2903–2906; b) Q. Ma, W. Zhuo, Z. Zhai, G. Gong, T. Zhang, H. Xiao, Z. Zhou, Y. Liu, *Spectrochim. Acta Part A* **2021**, *261*, 120031; c) C. G. Frankær, M. Rosenberg, M. Santella, K. J. Hussain, B. W. Laursen, T. J. Sørensen, *ACS Sens.* **2019**, *4*, 764–773.
[6] a) F. Le Guern, V. Mussard, A. Gaucher, M. Rottman, D. Prim, *Int. J. Mol. Sci.* **2020**, *21*, 9217; b) Y. Koide, R. Kojima, K. Hanaoka, K. Numasawa, T. Komatsu, T. Nagano, H. Kobayashi, Y. Urano, *Commun. Chem.* **2019**, *2*, 94.
[7] a) A. H. Romero, H. E. Cerecetto, *J. Org. Chem.* **2022**, *87*, 7618–7634; b) H. J. Park, C. S. Lim, E. S. Kim, J. H. Han, T. H. Lee, H. J. Chun, B. R. Cho, *Angew. Chem. Int. Ed.* **2012**, *51*, 2673–2676; c) T. Umeno, R. Seto, S. Matsumoto, M. Fujihara, S. Karasawa, *Anal. Chem.* **2022**, *94*, 10400–10407; d) S. Wang, Y. Fan, D. Li, C. Sun, Z. Lei, L. Lu, T. Wang, F. Zhang, *Nat. Commun.* **2019**, *10*, 1058.
[8] a) J. F. Ireland, P. A. H. Wyatt, *Adv. Phys. Org. Chem.* **1976**, *12*, 131–221; b) L. G. Arnaut, S. J. Formosinho, *J. Photochem. Photobiol. A* **1993**, *75*, 1–20; c) L. M. Tolbert, K. M. Solntsev, *Acc. Chem. Res.* **2002**, *35*, 19–27; d) N. Agmon, *J. Phys. Chem. A* **2005**, *109*, 13–35; e) T. Kumpulainen, B. Lang, A. Rosspeintner, E. Vauthey, *Chem. Rev.* **2017**, *117*, 10826–10939; f) M. Mohapatra, A. K. Mishra, *Photochem. Photobiol. Sci.* **2019**, *18*, 2830–2848; g) Y. Li, D. Dahal, C. S. Abeywickrama, Y. Pang, *ACS Omega* **2021**, *6*, 6547–6553; h) A. C. Sedgwick, L. Wu, H.-H. Han, S. D. Bull, X.-P. He, T. D. James, J. L. Sessler, B. Z. Tang, H. Tian, J. Yoon, *Chem. Soc. Rev.* **2018**, *47*, 8842–8880; i) H. C. Joshi, L. Antonov, *Molecules* **2021**, *26*, 1475.
[9] a) J. Saway, Z. M. Salem, J. J. Badillo, *Synthesis* **2020**, *53*, 489–497; b) H. Kagel, M. Frohme, J. Glökler, *J. Cell. Biotechnol.* **2018**, *4*, 23–30; c) Y. Liao, *Phys. Chem. Chem. Phys.* **2022**, *24*, 4116–4124; d) R. Nandi, N. Amdursky, *Acc. Chem. Res.* **2022**, *55*, 2728–2739; e) M. J. Voegtle, J. M. Dawlaty, *J. Am. Chem. Soc.* **2022**, *144*, 8178–8184.
[10] A. Yucknovsky, Y. Shlosberg, N. Adir, N. Amdursky, *Angew. Chem. Int. Ed.* **2023**, *62*, e202301541.
[11] X. Zhang, S. Hu, Q. Ma, S. Liao, *Polym. Chem.* **2020**, *11*, 3709–3715.
[12] A. Das, S. Ayad, K. Hanson, *Org. Lett.* **2016**, *18*, 5416–5419.
[13] L. H. Leijendekker, J. Weweler, T. M. Leuther, D. Kratzert, J. Streuff, *Chem. Eur. J.* **2019**, *25*, 3382–3390.
[14] C. Reichardt, T. Welton, in *Solvents and Solvent Effects in Organic Chemistry*, Wiley-VCH, Weinheim, **2010**, pp. 359–424.
[15] E. Bosch, M. Rosés, *J. Chem. Soc. Faraday Trans.* **1992**, *88*, 3541–3546.
[16] a) R. A. Shagidullina, I. S. Ryzhkina, A. B. Mirgorodskaya, L. A. Kudryavtseva, V. E. Bel'skii, B. E. Ivanov, *Russ. Chem. Bull.* **1994**, *43*, 1149–1152; b) T. Yamashita, H. Yano, S. Harada, T. Yasunaga, *J. Phys. Chem.* **1984**, *88*, 2671–2674; c) T. Yamashita, M. Sumino, H. Yano, S. Harada, T. Yasunaga, *Bull. Chem. Soc. Jpn.* **1984**, *57*, 2352–2356.
[17] S. Doloczki, C. Kern, K. Holmberg, F. Swartling, J. Streuff, C. Dyrager, *Chem. Eur. J.* **2023**, e202300864.
[18] a) B. Marciniak, H. Kozubek, S. Paszyc, *J. Chem. Educ.* **1992**, *69*, 247–249; b) W. Sheng, M. Nairat, P. D. Pawlaczyk, E. Mroczka, B. Farris, E. Pines, J. H. Geiger, B. Borhan, M. Dantus, *Angew. Chem. Int. Ed.* **2018**, *57*, 14742–14746.

[19] a) A. Jiménez-Sánchez, R. Santillan, *Analyst* **2016**, *141*, 4108–4120; b) E. W. Driscoll, J. R. Hunt, J. M. Dawlaty, *J. Phys. Chem. Lett.* **2016**, *7*, 2093–2099.
[20] E. M. Santos, W. Sheng, R. Esmatpour Salmani, S. Tahmasebi Nick, A. Ghanbarpour, H. Gholami, C. Vasileiou, J. H. Geiger, B. Borhan, *J. Am. Chem. Soc.* **2021**, *143*, 15091–15102.
[21] a) P. Ballinger, F. A. Long, *J. Am. Chem. Soc.* **1960**, *82*, 795–798; b) P. Ballinger, F. A. Long, *J. Am. Chem. Soc.* **1959**, *81*, 1050–1053; c) R. W. Kingerley, V. K. LaMer, *J. Am. Chem. Soc.* **1941**, *63*, 3256–3262; d) D. C. Martin, J. A. V. Butler, *J. Chem. Soc.* **1939**, 1366–1369; e) C. K. Rule, V. K. L. Mer, *J. Am. Chem. Soc.* **1938**, *60*, 1974–1981; f) S. Korman, V. K. L. Mer, *J. Am. Chem. Soc.* **1936**, *58*, 1396–1403.
[22] a) L. Stryer, *J. Am. Chem. Soc.* **1966**, *88*, 5708–5712; b) H. Shizuka, *Acc. Chem. Res.* **1985**, *18*, 141–147.
[23] J. Maillard, K. Klehs, C. Rumble, E. Vauthey, M. Heilemann, A. Fürstenberg, *Chem. Sci.* **2021**, *12*, 1352–1362.
[24] J. R. Hunt, J. M. Dawlaty, *J. Phys. Chem. A* **2018**, *122*, 7931–7940.
[25] J. Lahiri, M. Moemeni, J. Kline, B. Borhan, I. Magoulas, S. H. Yuwono, P. Piecuch, J. E. Jackson, M. Dantus, G. J. Blanchard, *J. Phys. Chem. B* **2019**, *123*, 8448–8456.
[26] R. B. Grossman, in *The Art of Writing Reasonable Organic Reaction Mechanisms*, Springer Cham, **2019**.
[27] a) B. A. Webb, F. M. Aloisio, R. A. Charafeddine, J. Cook, T. Wittmann, D. L. Barber, *Mol. Biol. Cell* **2021**, *32*, 131–142; b) D. E. Johnson, P. Ostrowski, V. Jaumouillé, S. Grinstein, *J. Cell Biol.* **2016**, *212*, 677–692.
[28] G. R. Fulmer, A. J. M. Miller, N. H. Sherden, H. E. Gottlieb, A. Nudelman, B. M. Stoltz, J. E. Bercaw, K. I. Goldberg, *Organometallics* **2010**, *29*, 2176–2179.
[29] A. M. Brouwer, *Pure Appl. Chem.* **2011**, *83*, 2213–2228.
[30] H. T. S. Britton, R. A. Robinson, *J. Chem. Soc.* **1931**, 1456–1462.
[31] a) J. E. Whitaker, R. P. Haugland, F. G. Prendergast, *Anal. Biochem.* **1991**, *194*, 330–344; b) H. J. Kim, C. H. Heo, H. M. Kim, *J. Am. Chem. Soc.* **2013**, *135*, 17969–17977.
[32] M. J. Frisch, G. W. Trucks, H. B. Schlegel, G. E. Scuseria, M. A. Robb, J. R. Cheeseman, G. Scalmani, V. Barone, B. Mennucci, G. A. Petersson, H. Nakatsuji, M. Caricato, X. Li, H. P. Hratchian, A. F. Izmaylov, J. Bloino, G. Zheng, J. L. Sonnenberg, M. Hada, M. Ehara, K. Toyota, R. Fukuda, J. Hasegawa, M. Ishida, T. Nakajima, Y. Honda, O. Kitao, H. Nakai, T. Vreven, J. A. Montgomery Jr., J. E. Peralta, F. Ogliaro, M. Bearpark, J. J. Heyd, E. Brothers, K. N. Kudin, V. N. Staroverov, T. Keith, R. Kobayashi, J. Normand, K. Raghavachari, A. Rendell, J. C. Burant, S. S. Iyengar, J. Tomasi, M. Cossi, N. Rega, J. M. Millam, M. Klene, J. E. Knox, J. B. Cross, V. Bakken, C. Adamo, J. Jaramillo, R. Gomperts, R. E. Stratmann, O. Yazyev, A. J. Austin, R. Cammi, C. Pomelli, J. W. Ochterski, R. L. Martin, K. Morokuma, V. G. Zakrzewski, G. A. Voth, P. Salvador, J. J. Dannenberg, S. Dapprich, A. D. Daniels, O. Farkas, J. B. Foresman, J. V. Ortiz, J. Cioslowski, D. J. Fox, Gaussian 09, Revision D.01, Gaussian Inc., Wallingford CT, **2013**.
[33] D. Jacquemin, V. Wathelet, E. A. Perpète, C. Adamo, *J. Chem. Theory Comput.* **2009**, *5*, 2420–2435.
[34] a) M. D. Hanwell, D. E. Curtis, D. C. Lonie, T. Vandermeersch, E. Zurek, G. R. Hutchison, *J. Cheminf.* **2012**, *4*, 17; b) Avogadro: an open-source molecular builder and visualization tool. Version 1.2.0. https://avogadro.cc/.
[35] a) J. Schindelin, I. Arganda-Carreras, E. Frise, V. Kaynig, M. Longair, T. Pietzsch, S. Preibisch, C. Rueden, S. Saalfeld, B. Schmid, J.-Y. Tinevez, D. J. White, V. Hartenstein, K. Eliceiri, P. Tomancak, A. Cardona, *Nat. Methods* **2012**, *9*, 676–682; b) C. A. Schneider, W. S. Rasband, K. W. Eliceiri, *Nat. Methods* **2012**, *9*, 671–675.
[36] R. N. Majzoub, E. Wonder, K. K. Ewert, V. R. Kotamraju, T. Teesalu, C. R. Safinya, *J. Phys. Chem. B* **2016**, *120*, 6439–6453.
[37] S. Rondinini, P. Longhi, P. R. Mussini, T. Mussini, *Pure Appl. Chem.* **1987**, *59*, 1693–1702.

Manuscript received: August 2, 2023
Revised manuscript received: September 1, 2023
Accepted manuscript online: September 14, 2023
Version of record online: September 28, 2023